A Robust Light Use Efficiency Model Parameterization Method Based on Ecosystem Properties

Shanning Bao[1,2*], Lazaro Alonso[1], Siyuan Wang[1], Johannes Gensheimer[1], Ranit De[1], Nuno Carvalhais[1,3*]

1. Department for Biogeochemical Integration, Max-Planck-Institute for Biogeochemistry, Jena, Germany

2. National Space Science Center, Chinese Academy of Sciences, Beijing, China

3. Departamento de Ciências e Engenharia do Ambiente, DCEA, Faculdade de Ciências e Tecnologia, FCT, Universidade Nova de Lisboa, 2829-516 Caparica, Portugal

([*]Corresponding authors: Shanning Bao, baoshanning@nssc.ac.cn, Nuno Carvalhais, ncarvalhais@bgc-jena.mpg.de)

Abstract

In a model simulating the dynamics of a system, parameters can represent system properties and unresolved processes, therefore affecting the model accuracy and uncertainties. For a light use efficiency (LUE) model, which is a typical tool to estimate gross primary productivity (GPP), the plant-functional-type (PFT)-dependent parameterization method was widely used to extrapolate parameters to larger spatial scales. However, the method cannot capture the spatial variability within PFT and introduces misclassification errors. Here we proposed an ecosystem-property-based parameterization method (mNN-GPP) for an LUE model to overcome the issues. This method refers to predicting model parameters using the multi-output artificial neural network based on collected variables including PFT, climate types, bioclimatic variables, vegetation features, atmospheric deposition and soil properties at 196 FLLUXNET eddy covariance flux sites. The neural network was optimized according to GPP errors and constraints on sensitivity functions of the LUE model. We compared mNN-GPP with eleven other typical parameter extrapolating methods, including PFT-, climate-specific parameterization, global and PFT-based parameter optimization, site-similarity-based, and regression methods. These twelve methods were assessed using Nash-Sutcliffe model efficiency (NSE), determination coefficient and normalized root mean squared error of the simulated GPP. The simulated results were also contrasted with those of site-specific calibration based on full-time-series GPP estimated from observational net ecosystem exchange. The N-fold cross-validated results showed that mNN-GPP had the best performance across various temporal and spatial scales (e.g., NSE=0.62 at the daily scale). No extrapolated parameters reached the same performance as the calibrated parameters (NSE=0.82), but the ranges of predicted parameters were constrained. Furthermore, the Shapley values, layer-wise relevance and partial dependence of the input features showed that bioclimatic variables, PFT, and vegetation features are the key variables determining parameters. We recommend using the parameterization method considering both ecosystem properties and prediction errors to other GPP models and across spatio-temporal scales.

Keywords: parameter extrapolation, gross primary productivity, site-specific parameterization, vegetation and climate features, feature importance, spatio-temporal scales

1. Introduction

Growing multi-model-based studies reveal that large uncertainties resulted from various model structures, driver data and parameters (Huntzinger et al., 2017; Medlyn, Robinson, Clement, & McMurtrie, 2005; Zheng et al., 2018) are remained in modeling global carbon cycle and system responses to environmental changes (Baldocchi, Ryu, & Keenan, 2016; Bloom, Exbrayat, Van Der Velde, Feng, & Williams, 2016; Piao et al., 2020). Although model parameters contribute to considerable uncertainties, most global vegetation models were parameterized using fixed, biome- or plant functional type (PFT)- based values, which cannot capture the spatial variability of carbon process (Bloom et al., 2016). The fixed and PFT-based parameterization were also widely used in and introduced uncertainties to gross primary productivity (GPP) models (Groenendijk et al., 2011; Ryu, Berry, & Baldocchi, 2019), including light use efficiency (LUE), leaf-scale-process-based, machine-learning and sun-induced fluorescence models (Frankenberg et al., 2011; Jung et al., 2011; Running et al., 2004; Tian et al., 2020; Zhang et al., 2012). A more robust and physically intuitive parameterization method is desired for constraining the global GPP estimation.

LUE models are typical tools for the estimation of GPP at a large scale and the global scale (Mahadevan et al., 2008; Potter et al., 1993; Running et al., 2004; Tian et al., 2020; Yuan et al., 2007). The kind of models incorporates the knowledge of environmental constraints to the originally proposed empirical LUE model, Monteith et al.'s model (Monteith, 1972), having advantages of high efficiency and algorithmic transparency compared to leaf-scale-process-based models and machine-learning-based models, respectively.

The first global GPP product based on MODIS LUE algorithm (Running et al., 2004) proposed a set of PFT-dependent parameters. Other later published global LUE models inherit the PFT-based parameterization method or parameters directly from papers (He et al., 2013; Mahadevan et al., 2008; Xiao et al., 2004; Xie & Li, 2020). However, applying parameters in regions which it was not previously used for or evaluated against might easily lead to the erroneous conclusion that a specific model structure and parameter set falls short in locally describing ecosystem GPP. To overcome this limitation, LUE modelers usually calibrate parameters in their physical ranges according to the distance to the observational GPP (Nuno Carvalhais et al., 2008; Horn & Schulz, 2011a; Mäkelä et al., 2008; Yan et al., 2017; Zhou et al., 2016), i.e., the GPP estimated from eddy covariance (EC) carbon flux. This method has to be supported by the availability of EC flux towers, was therefore unable to be used globally. To extrapolate parameters to regions without observations, Carvalhais et al parameterized the CASA model based on the inversed parameter vector at the EC site which has the same PFT and the most similar climate and vegetation features to the target region (N Carvalhais et al., 2010). Other studies select to use the average site-level optimized parameters per PFT (Guan, Chen, Shen, Xie, & Tan, 2022; Yuan, Cai, Xia, et al., 2014; Zhou et al., 2016), PFT-specific optimized parameters (Tian et al., 2020; Zheng et al., 2020), globally optimized parameters (Stocker et al., 2020; Yuan et al., 2019) or globally fixed parameters (Mengoli et al., 2022; H. Wang et al., 2017). Yuan et al showed using six different LUE models that the modeled GPP using globally optimized parameters was not significantly different from that using PFT-specific optimized parameters (Yuan, Cai, Liu, et al., 2014). A study afterwards based on PRELES model, nevertheless, illustrated that at least the variance in parameters across PFT needs to be considered to reach a promise model performance level (Tian et al., 2020). In general, most studies did not account variances of parameters within PFT, but all assumed that the LUE model parameters are related to detailed characteristics of the vegetation and the growing environment.

In some studies, the drivers for spatial changes of model parameters were analyzed based on the site-level calibrated parameters. For example, Horn et al (2011b) found that the parameters of a LUE model, which represent the maximum light use efficiency, the sensitivity of GPP to temperature and soil moisture, varied across climate zones and biomes and can be predicted using vegetation and environmental properties. The relationship between parameters and plant traits also existed in process-based GPP models (Peaucelle et al., 2019). Moreover, Luo et al (2020) claimed that model parameters, which can represent both the evolving ecosystem properties and the unresolved ecosystem processes, should be determined according to our knowledge about the changing ecosystem properties. These studies all confirmed the control of vegetation and environmental attributes on model parameters, which represents GPP sensitivities. These findings inspire the possible next generation of parameterization method based on the physical connection between model parameters and ecosystem properties.

In this study we aim to propose a new LUE model parameterization method (or parameter extrapolation method) and explore the drivers for the model parameters. Our hypothesis is that the PFT-based parameterization cannot perform as well as the site-specific parameterization. We assume that the spatial variations of parameters, indicating the GPP sensitivities to environmental forcings, can be predicted by the ecosystem properties. To test the hypotheses, we compared 12 different parameterization methods based on a LUE model with appropriate environmental drivers and sensitivity functional forms selected from an ensemble of 5600 LUE models (Bao et al., 2022). These parameterization methods were assessed according to the accuracy of the simulated GPP (GPP_{sim}) across different time scales at the site-level, per PFT, per climate type and globally. The neural-network-based method taking GPP as the fitting target (see the method in section 2.4.6) reach the highest performance and is recommended by our study to be applied at other spatio-temporal scales and for other kinds of vegetation models.

2. Method

2.1 Light use efficiency model

LUE models define GPP as a product of the photosynthetically active radiation (PAR), the fraction of photosynthetically active radiation (FAPAR) and the maximum light use efficiency ($\boldsymbol{\varepsilon}_{\mathbf{max}}$), regulated by environmental sensitivity functions. The environmental drivers and sensitivity functional forms differ across LUE models. To minimize the effect of the selection of environmental drivers and sensitivity functions, we select a LUE model based on a model evaluation study (Bao et al., 2022) which considers the impacts of temperature (T), vapor pressure deficit (VPD), atmospheric CO_2 concentration (c_a), soil moisture (W), light intensity (L) and cloudiness index (CI) on GPP dynamics (see equations 1-8).

$$\mathrm{GPP}=\mathrm{PAR}\cdot\mathrm{FAPAR}\cdot\boldsymbol{\varepsilon}_{\mathbf{max}}\cdot f\mathrm{T}\cdot f\mathrm{VPD}\cdot f\mathrm{W}\cdot f\mathrm{L}\cdot f\mathrm{CI} \tag{1}$$

$$f\mathrm{T}=\frac{2e^{-\left(\mathrm{T_f}-\mathbf{T_{opt}}\right)/\mathbf{k_T}}}{1+e^{\left(-\left(\mathrm{T_f}-\mathbf{T_{opt}}\right)/\mathbf{k_T}\right)^2}} \tag{2}$$

$$f\mathrm{VPD}=e^{\boldsymbol{\kappa}\left(\frac{\mathbf{C_{a0}}}{\mathrm{c_a}}\right)^{\mathbf{C}_{\boldsymbol{\kappa}}}\mathrm{VPD}}\left(1+\frac{\mathrm{c_a}-\mathbf{C_{a0}}}{\mathrm{c_a}-\mathbf{C_{a0}}+\mathbf{C_m}}\right) \tag{3}$$

$$f\mathrm{W}=\frac{1}{1+e^{\mathbf{k_W}\left(\mathbf{k_W}-\mathbf{W_I}\right)}} \tag{4}$$

$$f\mathrm{L}=\frac{1}{1+\boldsymbol{\gamma}\cdot\mathrm{APAR}} \tag{5}$$

$$f\mathrm{CI}=\mathrm{CI}^{\boldsymbol{\mu}} \tag{6}$$

$$\mathrm{T_f}(t)=(1-\boldsymbol{\alpha}_{\mathbf{T}})\cdot\mathrm{T}(t)+\boldsymbol{\alpha}_{\mathbf{T}}\cdot\mathrm{T_f}(t-1) \tag{7}$$

$$\mathrm{T_f}(t)=(1-\boldsymbol{\alpha}_{\mathbf{W}})\cdot\mathrm{W}(t)+\boldsymbol{\alpha}_{\mathbf{W}}\cdot\mathrm{W_f}(t-1) \tag{8}$$

The LUE model includes thirteen parameters (in **bold**) in total. All sensitivity functions (*f*T, *f*VPD, *f*W, *f*L and *f*CI) are scaled from zero to one, representing from strong to no constraints. The physical meanings and units of the parameters and references of these sensitivity functions are summarized in Table 1. The sensitivity function of VPD, *f*VPD, includes the effect of both VPD and c_a, which jointly control the leaf internal CO_2 concentration. The pure CO_2 fertilization effect is described only by the right part of *f*VPD (i.e., the summary of one and c_a function). The product of PAR and FAPAR, the absorbed photosynthetically active radiation (APAR), is the estimate of the light energy intercepted by the vegetation canopy, thus was used as the light intensity input of the sensitivity function of L (*f*L). The T and W were temporally filtered using the lag parameters, $\boldsymbol{\alpha}_{\mathbf{T}}$ and $\boldsymbol{\alpha}_{\mathbf{W}}$, at boreal and arid regions, respectively.

Table 1. List of LUE model parameters

Parameters	Meanings	Range	Units	References
$\boldsymbol{\varepsilon}_{\mathbf{max}}$	Maximum light use efficiency	0 - 10	$gC\cdot MJ^{-1}$	(Running et al., 2004)
$\mathbf{T_{opt}}$	Optimal temperature	5 - 35	°C	(Horn & Schulz, 2011a)

$\mathbf{k_T}$	Sensitivity to temperature changes	1 - 20	-	As above
$\boldsymbol{\kappa}$	Sensitivity to vapor pressure deficit changes	-10^{-1} - -10^{-4}	kPa^{-1}	(Mäkelä et al., 2008)
$\mathbf{C_{a0}}$	Minimum optimal atmospheric CO_2 concentration	340 – 390	ppm	(Kalliokoski, Makela, Fronzek, Minunno, & Peltoniemi, 2018)
$\mathbf{C_\kappa}$	Sensitivity to atmospheric CO_2 concentration changes	0 – 10	-	As above
$\mathbf{C_m}$	CO_2 fertilization intensity indicator	100 – 4000	ppm	As above
$\mathbf{k_W}$	Sensitivity to soil moisture changes	-30 - -5	-	(Horn & Schulz, 2011a)
$\mathbf{W_I}$	Optimal soil moisture	0.01 – 0.99	$cm \cdot cm^{-1}$	As above
$\boldsymbol{\gamma}$	Light saturation curvature indicator	0 - 1	$MJ^{-1} \cdot m^2 \cdot d$	(Mäkelä et al., 2008)
$\boldsymbol{\mu}$	Sensitivity to cloudiness index changes	10^{-3} - 1	-	(Bao et al., 2022)
$\boldsymbol{\alpha_T}$	Lag parameter for temperature effect	0.0 - 0.9	-	(Horn & Schulz, 2011a)
$\boldsymbol{\alpha_W}$	Lag parameter for soil moisture effect	0.0 - 0.9	-	As above

2.2 Light use efficiency model forcings and calibrated parameters

The forcing data for the LUE model were collected at 196 EC sites (listed in Table S1) from FLUXNET (www.fluxnet.org). The detailed sources and algorithms of the forcing data are summarized in Table S2. The GPP estimated from the observed net ecosystem exchange (NEE) at EC sites (GPP_{obs}) were also collected to calibrate parameters (see the details about parameter calibration in section S1) and evaluate parameterization methods. We considered the simulated GPP using calibrated parameters (GPP_{calib}) as a reference for its good fitness to GPP_{obs}. As a derivative-free global searching algorithm, CMAES (Hansen & Kern, 2004), was used to calibrate parameters in its physical range according to the full time series of GPP_{obs}, we assumed that GPP_{calib} can reach the model potential (i.e., highest model performance).

2.3 Input features for predicting parameters

To extrapolate the parameters to the global scale, we collect mainly the variables that can represent the ecosystem properties available at both local (i.e., site-level) and global scales. These variables include the PFT, climate classification types, nineteen bioclimatic variables (BIO1-19), two aridity features (AI1-2), eleven vegetation features (VIF1-11), atmospheric Nitrogen and Phosphorus deposition ($Ndep_{NHX}$, $Ndep_{NOY}$, Pdep) and seventeen soil properties (Table 2).

Table 2. List of the input features for predicting parameters

Class name	Short names	Definitions	References
PFT	PFT	Plant functional types	See Table S1, eleven types in total
Clim	Clim	Koeppen-Geiger climate classification types	See Table S1, five main climate types and fourteen specific classification types in total
BioClim	BIO1	Annual Mean Temperature	Calculated based on the ANUCLIM algorithm (Xu & Hutchinson, 2011) using CRUNCEP dataset (Viovy, 2018) from 1986-2015.
	BIO2	Mean Diurnal Range (Mean of monthly maximum temperature minus minimum temperature)	
	BIO3	Isothermality (BIO2 divided by BIO7 and 100)	
	BIO4	Temperature Seasonality (standard deviation of temperature multiply with 100)	
	BIO5	Max Temperature of Warmest Month	
	BIO6	Min Temperature of Coldest Month	
	BIO7	Temperature Annual Range (BIO5 minus BIO6)	
	BIO8	Mean Temperature of Wettest Quarter	
	BIO9	Mean Temperature of Driest Quarter	
	BIO10	Mean Temperature of Warmest Quarter	
	BIO11	Mean Temperature of Coldest Quarter	
	BIO12	Annual Precipitation	
	BIO13	Precipitation of Wettest Month	
	BIO14	Precipitation of Driest Month	
	BIO15	Precipitation Seasonality (Coefficient of Variation)	
	BIO16	Precipitation of Wettest Quarter	
	BIO17	Precipitation of Driest Quarter	
	BIO18	Precipitation of Warmest Quarter	
	BIO19	Precipitation of Coldest Quarter	
	AI1	Mean annual aridity index (ratio between mean annual precipitation and potential evapotranspiration)	Calculated using the CRUNCEP dataset from 1986-2015
	AI2	Seasonality of aridity index (standard deviation of mean monthly aridity index)	
VIF	VIF1	Annual mean EVI (enhanced vegetation index)	Calculated based on the bioclimatic variables (BIO1-BIO11) algorithm using the gap-filled Landsat-based EVI (Walther et al., 2022) from 1986-2015
	VIF2	Mean monthly EVI range	
	VIF3	Mean EVI variability (VIF2 divided by VIF7)	
	VIF4	EVI seasonality (standard deviation of EVI)	
	VIF5	Max EVI of Warmest Month	
	VIF6	Min EVI of Coldest Month	

	VIF7	Annual EVI Range (BIO5 minus BIO6)	
	VIF8	Mean EVI of Wettest Quarter	
	VIF9	Mean EVI of Driest Quarter	
	VIF10	Mean EVI of Warmest Quarter	
	VIF11	Mean EVI of Coldest Quarter	
NPdep	$Ndep_{NHX}$	Average atmospheric nitrogen deposition (NH_3 and NH_4)	Extracted from the product of the atmospheric chemistry transport model TM3 (R. Wang et al., 2017)
	$Ndep_{NOY}$	Average atmospheric nitrogen deposition (NO and NO_2)	
	Pdep	Average atmospheric phosphorus deposition	
Soil	BDRICM	Depth to bedrock (R horizon) up to 200 cm	Extracted from the Soil Grids product (de Sousa et al., 2020)
	BDRLOG	Probability of occurrence (0-100%) of R horizon	
	BDTICM	Absolute depth to bedrock (in cm)	
	BLDFIE	Bulk density (fine earth) in kg/m3 at depth 0.00 m	
	CECSOL	Cation exchange capacity of soil in cmol/kg at depth 0.00 m	
	CLYPPT	Clay content (0-2 micro meter) mass fraction in % at depth 0.00 m	
	CRFVOL	Coarse fragments volumetric in % at depth 0.00 m	
	ORCDRC	Soil organic carbon content (fine earth fraction) in g/kg at depth 0.00 m	
	PHIHOX	Soil pH*10 in H2O at depth 0.00 m	
	PHIKCL	Soil PH (mulity with 10) in KCl at depth 0.00 m	
	SLTPPT	Silt content (2-50 micro meter) mass fraction in % at depth 0.00 m	
	SNDPPT	Sand content (50-2000 micro meter) mass fraction in % at depth 0.00 m	
	AWCh1	Derived available soil water capacity (volumetric fraction) with FC = pF 2.0 for depth 0 cm	
	AWCh2	Derived available soil water capacity (volumetric fraction) with FC = pF 2.3 for depth 0 cm	
	AWCh3	Derived available soil water capacity (volumetric fraction) with FC = pF 2.5 for depth 0 cm	
	WWP	Derived available soil water capacity (volumetric fraction) until wilting point for depth 0 cm	
	AWCtS	Saturated water content (volumetric fraction) teta-S for depth 0 cm	

The categorical variables (PFT and climate types) were converted to one or zero to indicate whether the target location belongs to a specific type or not. All non-categorical variables were normalized by subtracting the mean of each feature and a division by the standard deviation (equation 9). The normalized feature and original features are represented by *var* and var_{nor}. The mean and standard deviation per feature are represented by *mean* and *std*.

$$var_{\mathrm{nor}}=\frac{var\text{-}mean}{std} \tag{9}$$

2.4 Parameterization methods

We extrapolate the parameters based on N-fold cross-validation strategy using the collected ecosystem property variables. In other word, the samples, here refers to the EC sites, were divided into ten groups randomly (see the group number of each site in Table S1). We trained every time the parameterization models using nine of ten groups and validate the result using the left one group, and repeated ten times until getting validated results of all sites. All PFT and climate classification types (eleven PFT and fourteen climate classification types in total, see Table S1) were included in each training dataset.

The twelve parameterization methods can be divided into six groups (see details in section 2.4.1-2.4.5).

2.4.1 Arithmetic methods (‘$\mathrm{PFT_{mean}}$’, ‘$\mathrm{Clim_{mean}}$’, ‘$\mathrm{PFT_{med}}$’, and ‘$\mathrm{Clim_{med}}$’)

In the regions without observational data, the parameters were decided by the arithmetic mean of the calibrated parameters at the sites with the same PFT (Guan et al., 2022; Yuan, Cai, Xia, et al., 2014; Zhou et al., 2016). Here we tested the methods of using the mean and median parameters per PFT and climate type.

‘$\mathrm{PFT_{mean}}$’: the mean of the calibrated parameter vectors per PFT;

‘$\mathrm{Clim_{mean}}$’: the mean of the calibrated parameter vectors per main climate type;

‘$\mathrm{PFT_{med}}$’: the median of the calibrated parameter vectors per PFT;

‘$\mathrm{Clim_{med}}$’: the median of the calibrated parameter vectors per main climate type.

2.4.2 Similarity-based method (‘$\mathrm{PFT_{sim}}$’)

The site similarity is defined by Carvalhais et al.(2010) which measures the similarity (D) of the ecosystem properties between site *i* and site *j* as equation 10:

$$\mathrm{D}_{i,j}=1-\frac{\sum_{n=1}^{\mathrm{N}}\left(\boldsymbol{V}_{i,n}-\boldsymbol{V}_{j,n}\right)^2}{\sum_{n=1}^{\mathrm{N}}\left(\boldsymbol{V}_{i,n}-\overline{\boldsymbol{V}}_{i}\right)^2} \tag{10}$$

Here, $\boldsymbol{V}$ is a vector including the normalized daily mean of the air temperature, precipitation (in logarithm), global radiation and LANDSAT-based normalized difference vegetation index (NDVI, see data source and processing method in Table S2) between 1986 and 2015.

To determine the parameters of a target location, we calculated the D to each training site within the same PFT as the target location. The parameter vector at the site with the maximum D was used.

'PFT_{sim}': parameter vectors for each site from the most similar site.

2.4.3 Optimization-based methods ('OPT-All' and 'OPT-PFT')

The parameters can be optimized across all sites or at sites per PFT (Yuan, Cai, Liu, et al., 2014). Here we adopted the same algorithm, CMAES, and the same cost functions as the site-specific calibration method (see section S1).

'OPT-All': a parameter vector optimized using all sites in the training dataset.

'OPT-PFT': parameter vectors per PFT optimized using the sites within the same PFT in the training dataset.

2.4.4 Regression-based methods ('sRF', 'mRF', 'mNN-Par')

To test the assumption that the calibrated parameters are determined by the ecosystem properties, we here predict the calibrated parameters using the normalized features based on different regression methods.

'sRF': parameter vectors per site of which each parameter was predicted sequentially based on the single-output random forest (trees number=100; Breiman, 2001).

'mRF': parameter vectors per site predicted simultaneously based on the multi-output random forest (trees number=100; Pedregosa et al., 2011).

'mNN-Par': parameter vectors per site predicted simultaneously based on the multi-layer perceptron neural network (hidden layers number=2, neurons number=16; Gardner & Dorling, 1998; McCulloch & Pitts, 1943).

2.4.5 GPP-targeting method ('mNN-GPP')

Due to the model equifinality problem, which means different parameter vectors might result in the same model performance, the calibrated parameters might not represent the true parameters which reflect the GPP sensitivities controlled by the environmental properties. Here we additionally test the assumption that the ecosystem-properties-predicted parameter vector which might differ from the calibrated parameter vector can simulate GPP with a good accuracy. Instead of directly predicting parameters, we applied the neural network to predict GPP based on the LUE model using parameters predicted by the input features. The flowchart of this method is as Figure 1.

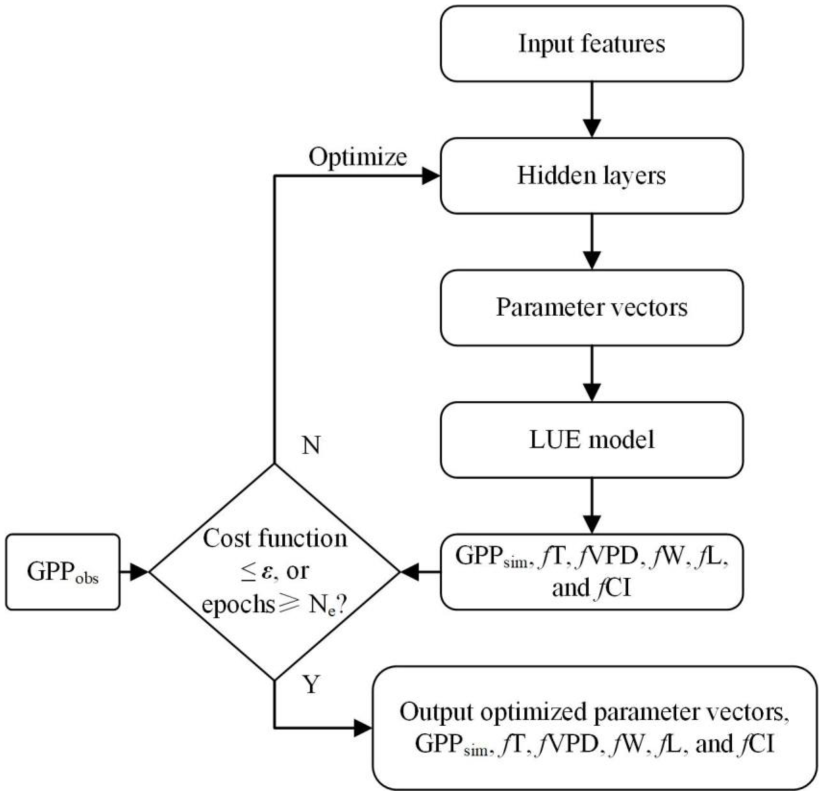

Figure 1. Flowchart of the GPP-targeting method. The parameter vectors per site are optimized until the cost function (see the definition in section S2) is lower than the threshold ($\boldsymbol{\varepsilon}$=10^{-2}) or epochs is more than the maximum epochs (=2×10^3).

At the first step, the neural network predicts the parameter vectors based on the normalized features. The GPP_{sim} is then simulated using the predicted parameter vectors and compared with GPP_{obs} to measure the model error (see the definition in section S2). The neural network back-propagates the error to each hidden layer and optimizes the weight and bias of each neuron based on ADAM algorithm (Kingma & Ba, 2014). We repeated the optimization process until the epochs reach 2×10^3. To overcome the overfitting problem, we set the learning rate (=10^{-3}), L_2 regularization coefficient (=10^{-4}), mini batch size (=32), neurons per layer (=16) and hidden layers (=2) according to a grid-searching experiment (not shown here). We further applied the drop-out strategy (Srivastava, Hinton, Krizhevsky, Sutskever, & Salakhutdinov, 2014) on the input and hidden layers. The outputs of the network include the simulated GPP, sensitivity functions and predicted parameter vectors per site.

'mNN-GPP': parameter vectors per site predicted using the multi-layer perceptron neural network on the target of minimizing GPP errors.

2.4.6 Globally-fixed method ('P-model')

P-model (Stocker et al., 2020; H. Wang et al., 2017) derived based on Farquhar et al (1980) and Fick's law together with an optimality theory (Prentice, Dong, Gleason, Maire, & Wright, 2014) adopts a globally-fixed parameter vector upscaled from the leaf-scale process. Mengoli et al (2022) improved the model by adding an acclimation process for the photosynthetic parameters. Here we ran Mengoli model based on the daily data, which is the same as the inputs for the other parameterization methods (section 2.2), using the initial parameters given in the paper and compared the model outputs, GPP, with other methods.

'P-model': a globally-fixed parameter vector from paper.

2.5 Statistical analysis for parameterized results

All the parameterization methods were assessed according to the GPP accuracy measured by Nash-Sutcliffe model efficiency (NSE, -∞-1; NSE=1 indicates a perfect model), determination coefficient (R^2, 0-1; R^2=1 indicates a perfect model) and normalized root mean squared error (NRMSE, 0-∞; NRMSE=0 indicates a perfect model) which is equal to the root mean squared error divided by the mean observational variable. Only good-quality data were used to calculate NSE, R^2 and NRMSE. Here the good-quality data refers to the input vector that the relevant quality flags (see 'QA' in Table S2) of all forcing data, GPP_{obs}, represented by the quality of NEE, are higher than 0.8 at the daily scale. When aggregated to longer time scales, the good quality data means the average quality flags are all higher than 0.7 at the weekly and monthly scales, and 0.5 at the yearly scale. Besides, the predicted parameters were compared to the calibrated parameters to test if the model equifinality problem exists.

2.5.1 Site-level temporal GPP assessment

We forced the LUE model at the daily scale and got the daily GPP_{sim} as a result. The weekly, monthly and yearly GPP_{sim} and GPP_{obs} were calculated based on the mean daily GPP_{sim} and GPP_{obs}, respectively. These time series of site-level GPP at different time scales were evaluated using NSE, R^2 and NRMSE. The vectors of NSE, R^2 and NRMSE were compared per PFT and climate types.

2.5.2 Spatial variability of GPP assessment

The site-mean GPP_{obs} across sites represent the spatial variance of GPP. We used NSE, R^2 and NRMSE to measure the accuracy of the site-mean GPP_{sim} compared with GPP_{obs} to evaluate the ability of the parameterization methods to capture the spatial variability of GPP.

2.5.3 Comprehensive assessment across spatio-temporal scales based on model likelihood

The likelihood of each parameterization method, ***P***, was calculated according to Bao et al (2022). To avoid selecting a method falling shortly in locally describing ecosystem GPP, ***P*** represents an overall performance at 200 different site groups. In every group, 100 sites were selected randomly from all sites and two site-years were then randomly extracted from each of these 100 sites. The 200 site-years GPP_{sim} were compared to GPP_{obs} based on NSE, R^2 and NRMSE at each site-year. The differences between the daily, weekly, and monthly NSE, R^2 and NRSE vectors (with 200 elements) and the yearly NRMSE vectors per parameterization method were tested using Kolmogorov-Smirnov statistical and t tests. The method with statistically higher NSE, R^2 or lower NRNSE than others has the largest score (=1, otherwise =0) at each site group. In case that two or more methods were statistically equal and better than others, the NSE, R^2 or NRMSE across all site-years was additionally computed to sort the methods independently. ***P*** is equal to the average score across all site groups. The average ***P*** across different statistical metrics (NSE, R^2 and NRMSE) and time scales (daily, weekly, monthly and yearly) was used to detect the best parameterization method.

2.5.4 Comparison between predicted parameters and calibrated parameters

Since the thirteen parameters have different meanings and ranges, they were compared independently. The similarity between the predicted parameters using methods introduced in section 2.4 and the calibrated parameters based on the observational data (see section S1) was assessed using NSE, R^2 and NRMSE.

2.6 Feature importance estimation

We evaluated the importance of input features using three methods and select the most importance features based on the average normalized feature importance values.

2.6.1 Shapley-based feature importance (SHAP)

The Shapley value of a feature is calculated based on the deviation of the predicted parameter at a certain input from the average prediction (Lundberg & Lee, 2017), which represent the contribution of a feature to the output. Here SHAP is equal to the average absolute Shapley value across all inputs. The average SHAP across all cross-validation groups(Friedman, 2001) was used to assess the contribution of features for each parameter and all parameters.

2.6.2 Layer-wise-relevance-propagation-based feature importance (LRP)

The layer-wise relevance propagation refers to a strategy which allows to decompose the prediction of neural network over an input feature (Montavon, Binder, Lapuschkin, Samek, & Müller, 2019). It is usually used in deep classification neural network, here we applied LRP to assess a shallow regression neural network yet. We calculated the relevance vector according to Bach et al. (2015) and measured the feature importance according to the average relevance across different cross-validation groups.

2.6.3 Partial-dependence-based feature importance (PD)

We estimated the partial dependence of the prediction to each input feature based on Friedman's (2001) algorithm. The PD was measured according to the partial dependence, which is equal to the standard deviation of the partial dependence if the input feature is non-categorical variables, otherwise is equal to the one fourth of the absolute partial dependence range (Greenwell, Boehmke, & McCarthy, 2018).

3. Results

3.1 Temporal and spatial assessment

The parameterization method based on neural network aiming at minimizing GPP errors, mNN-GPP, had the best performance compared with other typical parameterization methods. All the assessing metrics at daily, weekly, monthly and yearly scales, NSE (Figure 2), R^2 (Figure S1) and NRMSE (Figure S2), showed that mNN-GPP was better at more sites (i.e., more bright color blocks in Figure 2). The spatial variability of GPP can be also better captured by mNN-GPP, which had higher NSE, R^2 and lower NRMSE measured by site-mean GPP_{obs} and GPP_{sim} (Figure 3). The accuracy of time series and site-mean GPP_{sim} using other methods were all significantly worse than mNN-GPP. Although mNN-GPP cannot perform as well as the site-specific calibration, it is the best parameter extrapolation method globally.

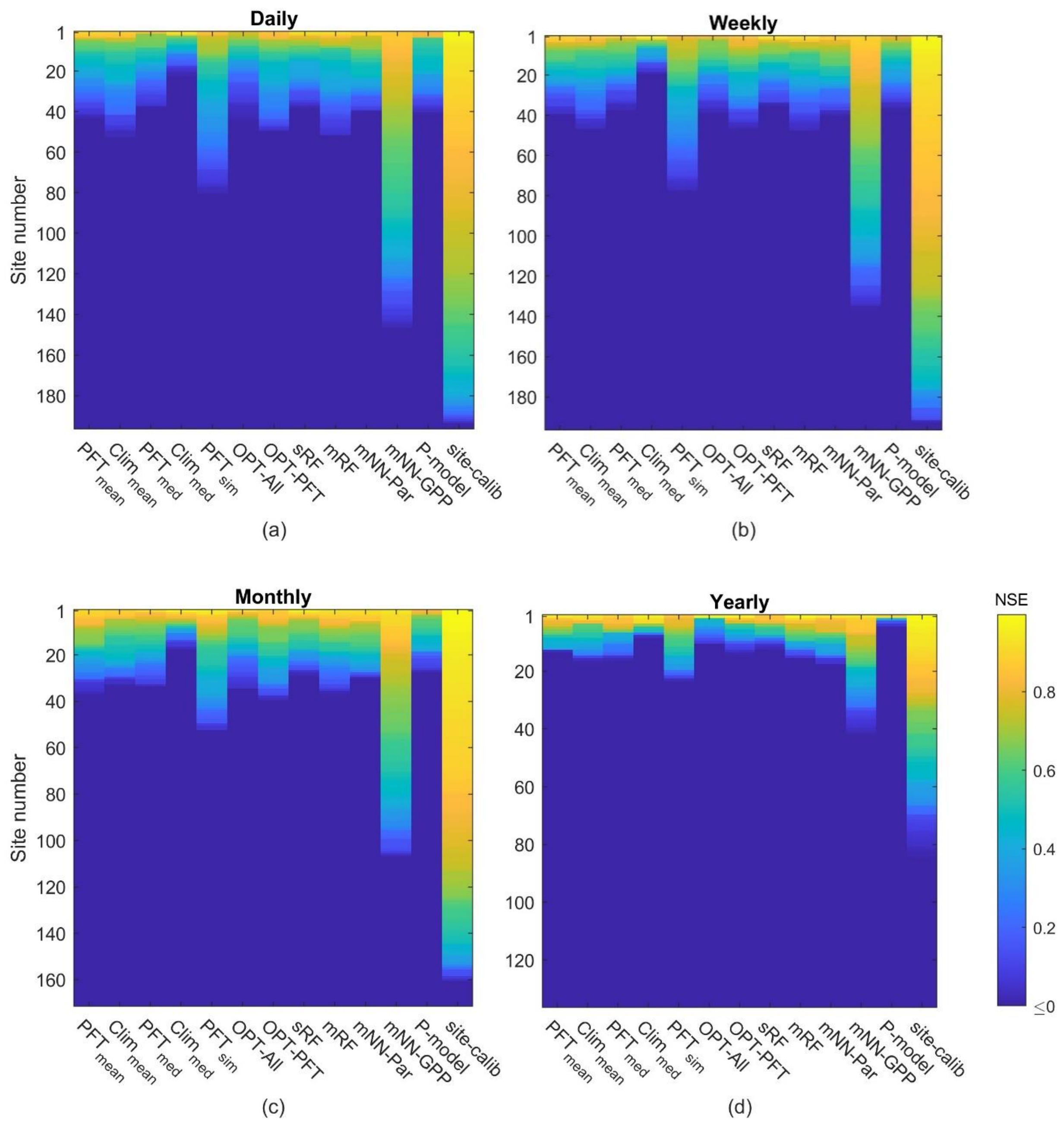

Figure 2. Comparison of NSE between GPP_{obs} and GPP_{sim} based on twelve different parameterization methods (see definitions of PFT_{mean}, $Clim_{mean}$, PFT_{med}, $Clim_{med}$, PFT_{sim}, OPT-All, OPT-PFT, sRF, mRF, mNN-Par, mNN-GPP, and P-model in section 2.4), and between GPP_{obs} and GPP_{calib} (site-calib, see the calibration process in section S1) at daily (a), weekly (b), monthly (c) and yearly (d) scales. The sites with less than four good-quality (defined in section 2.5) months or years were removed from penal c and d, respectively.

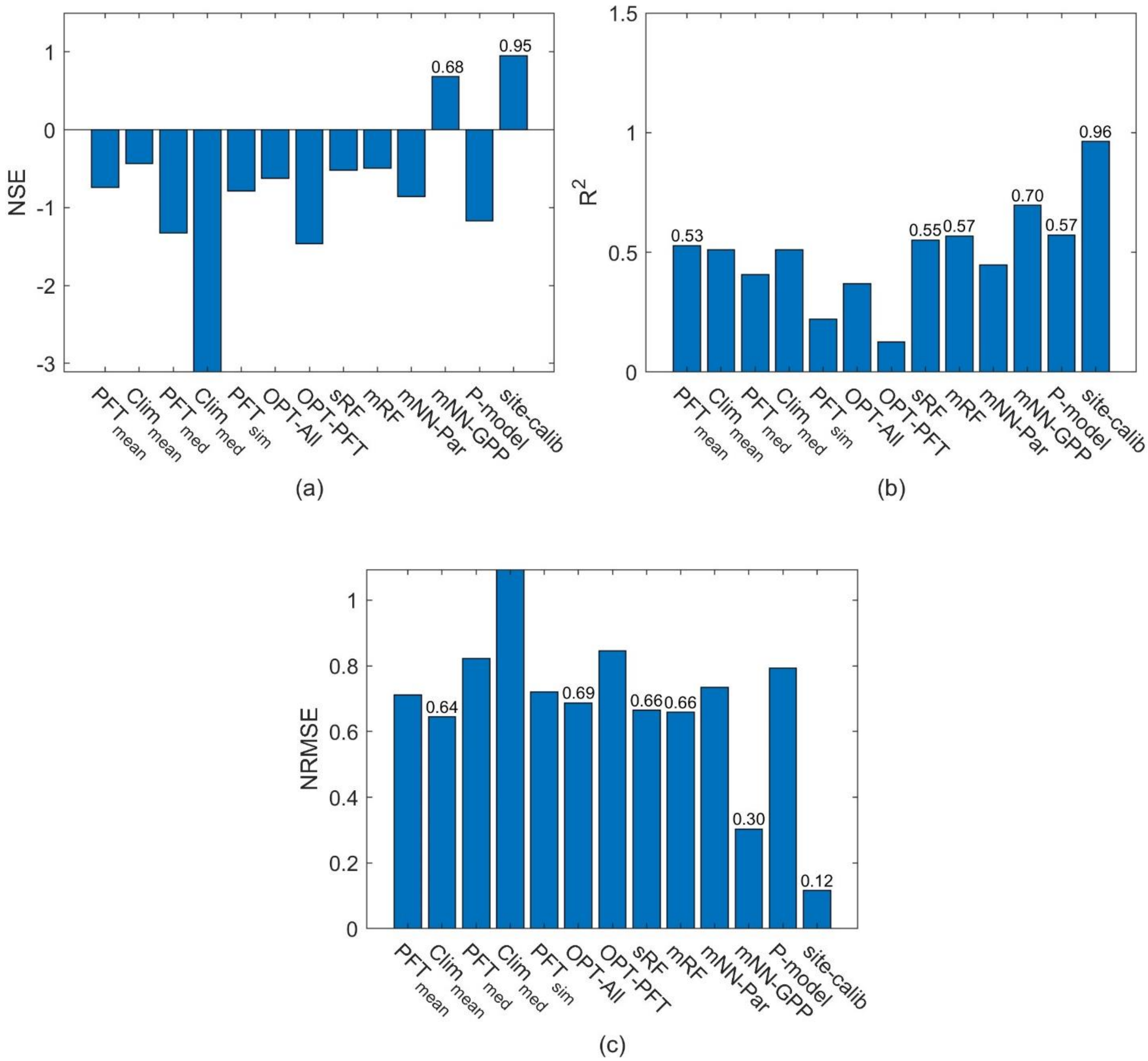

Figure 3. Comparison of NSE (a), R^2 (b), and NRMSE (c) between the site-mean GPP_{obs} and GPP_{sim}. The positive NSE, highest six R^2 and lowest six NRMSE values are displayed on the top of bars.

The global best parameterization method, mNN-GPP, outperformed across various PFT and climate types. It had the highest daily NSE quantiles for each PFT and climate type considered in this study (Figure 4). While mNN-GPP was relative better than other methods, no extrapolated parameters can provide accurate GPP dynamics (NSE>0.4) at closed shrubland (CSH in Figure 4a), tropical (A in Figure 4b) and polar (E in Figure

4b) climate types given that the model using calibrated parameters was good (grey colors in Figure 4). It demonstrated that the variance of current extrapolated parameters was still insufficient. Using R^2 or NRMSE as the assessing metric (Figure S3-4), the parameterization methods showed smaller but robust relative differences, i.e., the mNN-GPP was still the best method. In general, no extrapolated parameters can reach the highest model performance, mNN-GPP was the best option at areas without observational data.

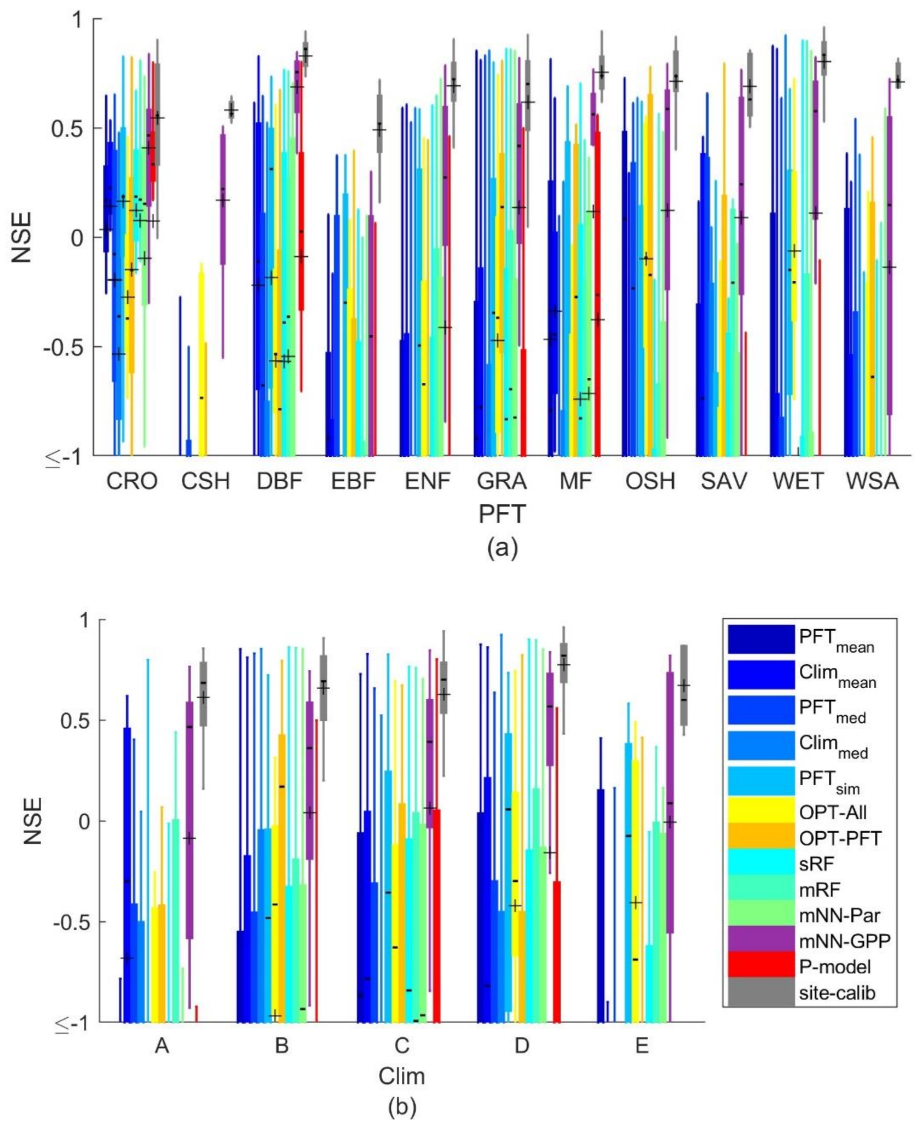

Figure 4. Site-level daily NSE comparison per plant functional type (a, PFT) and climate type (b, Clim). The mean and median per type are represented by the black cross and line, respectively. CRO=crop, CSH=closed shrubland, DBF=deciduous broadleaf forest, EBF=evergreen broadleaf forest, ENF=evergreen needleleaf forest, GRA=grass, MF=mixed forest, OSH=open shrubland, SAV=savanna, WET=wetland, WSA=woody savanna. A=tropic climate, B=arid climate, C=temperate climate, D=cold climate, E=polar climate

The model likelihood, ***P***, which represents the likelihood of a model statistically better than others across various site groups, illustrated that mNN-GPP was the best method to extrapolate parameters, following by OPT-All and $Clim_{med}$ with likelihoods lower than 0.06 (i.e., at less than 6% groups of sites the two methods can outperform). The average ***P*** of mNN-GPP across daily, weekly, monthly, and yearly scales, and across various assessing metrics was also significantly higher than the other methods. It represented that the method is robust across various temporal and spatial scales.

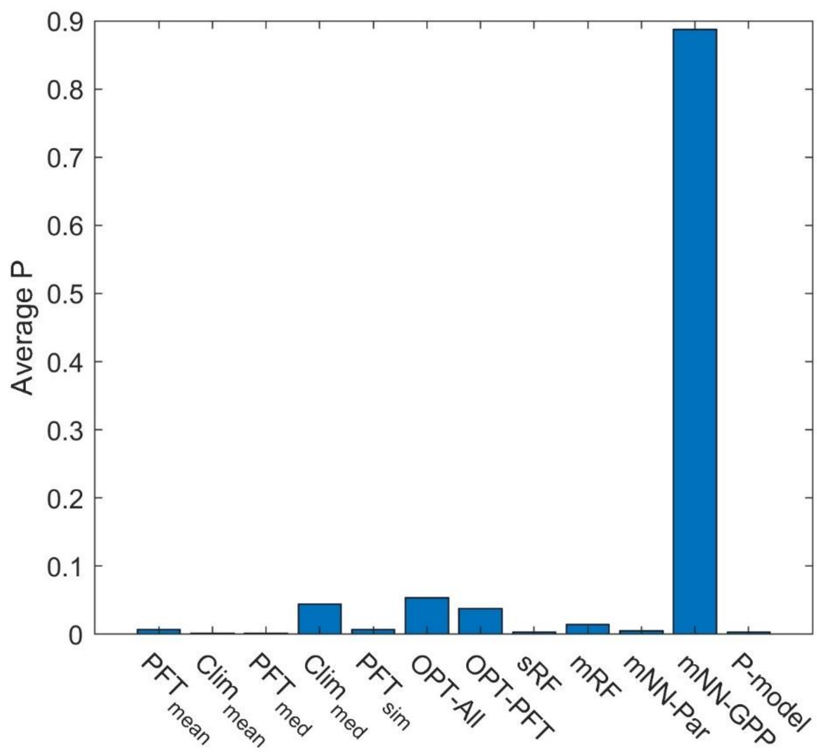

Figure 5. The average model likelihood (*P*) of parameterization methods

3.2 Difference between calibrated parameters and predicted parameters

The predicted parameters displayed different distribution pattern from the calibrated parameters. Taking the best method, mNN-GPP, as an example (Figure 6), the ranges of the predicted parameters were narrower than the calibrated parameters given the same predefined range. Further, the predicted parameters had no 'edge-hitting' problem, which means that the parameter frequently reaches its maximum or minimum values, e.g., the calibrated parameters T_{opt}, k_T, C_κ, C_{a0}, C_m and k_W (Figure 6b-c, f-h, j). The other parameterization methods also showed narrower ranges but no edge-hitting (e.g., mRF, $Clim_{med}$ and OPT-PFT in Figure S5-7). NSE between the predicted parameters using mNN-GPP and calibrated parameters across sites were all negative. The maximum R^2 was 0.08 and the lowest NRMSE was 0.08. Thus, the predicted parameters were not comparable to the calibrated parameters while they can produce similar GPP, highlighting the parameter equifinality in the LUE model.

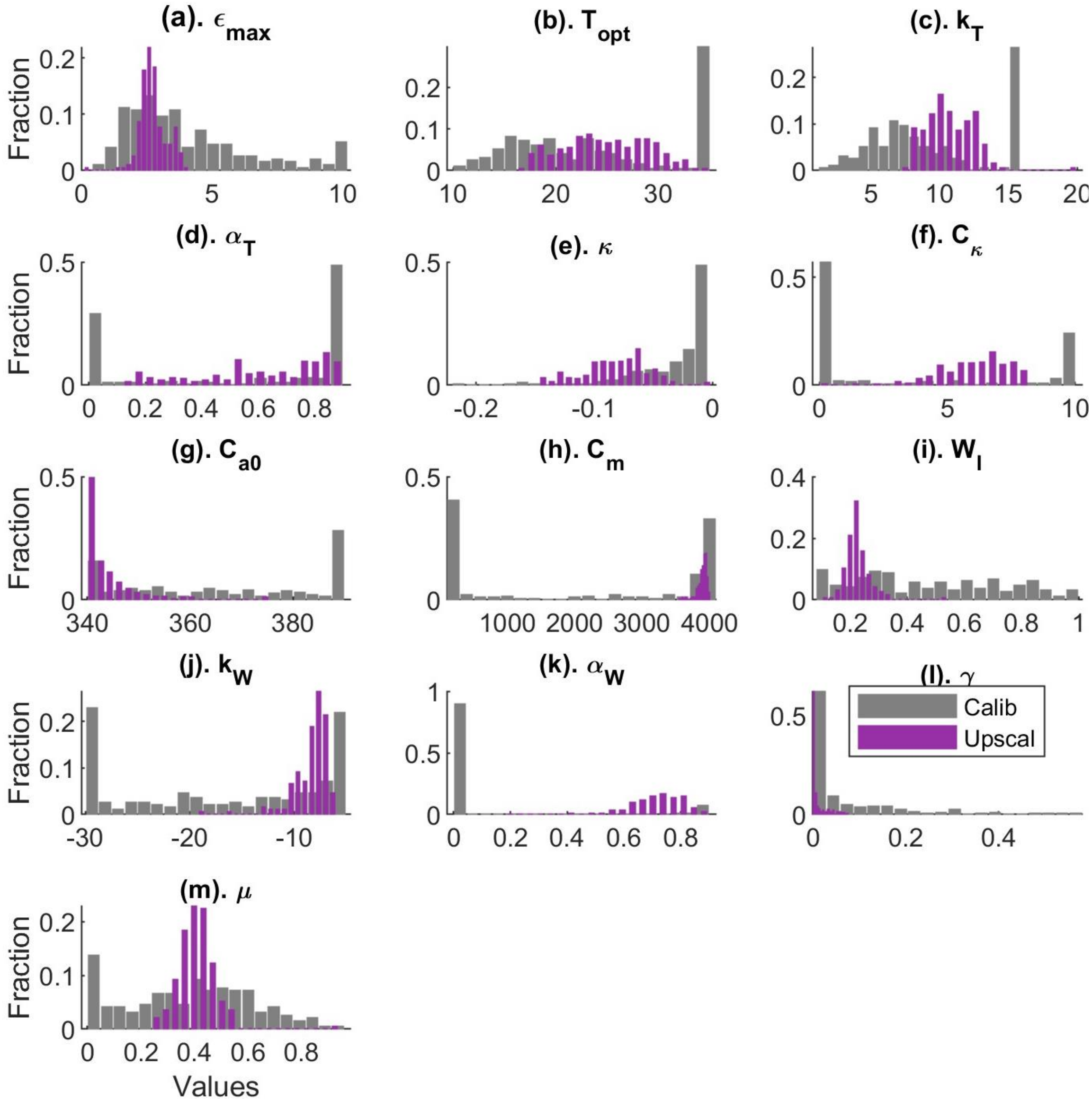

Figure 6. Distribution histogram of the calibrated parameters and the predicted parameters by mNN-GPP.

3.3 Important features for controlling model parameters

The average values of SHAP, LRP and PD illustrated that the bioclimate variables, PFT, and vegetation features were important features controlling spatial variability of parameters (Figure 7). The importance values differed across three different methods, but all of them showed that most climate types were not important for determining model parameters. Most bioclimate variables were shown to have higher importance than other features. The SHAP and LRP of most PFT were higher than other features. For a specific parameter, the most importance feature was not the same as the one for all parameters. For example, ε_{max} was controlled mainly by AI1 (mean annual aridity index, see figure S8) , nonetheless W_I was controlled primarily by VIF7 (the range of mean annual

EVI, see figure S9). In general, the bioclimate, PFT and vegetation features are determining the parameters which represent the GPP sensitivities to environment changes.

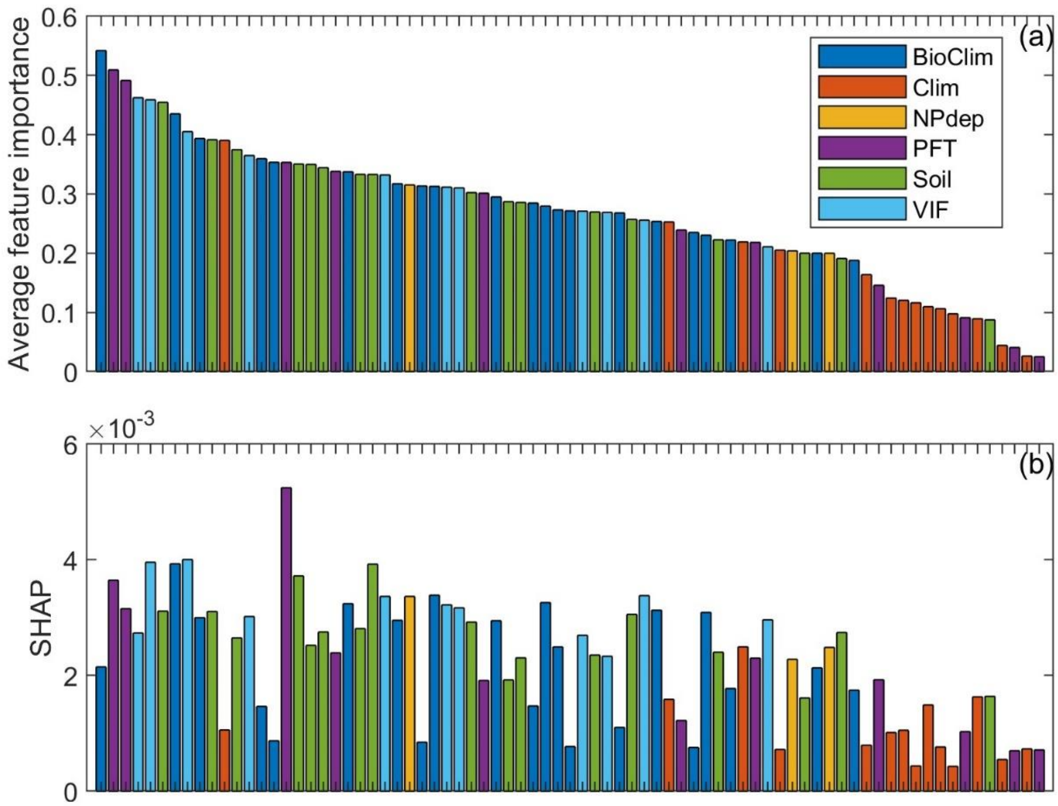

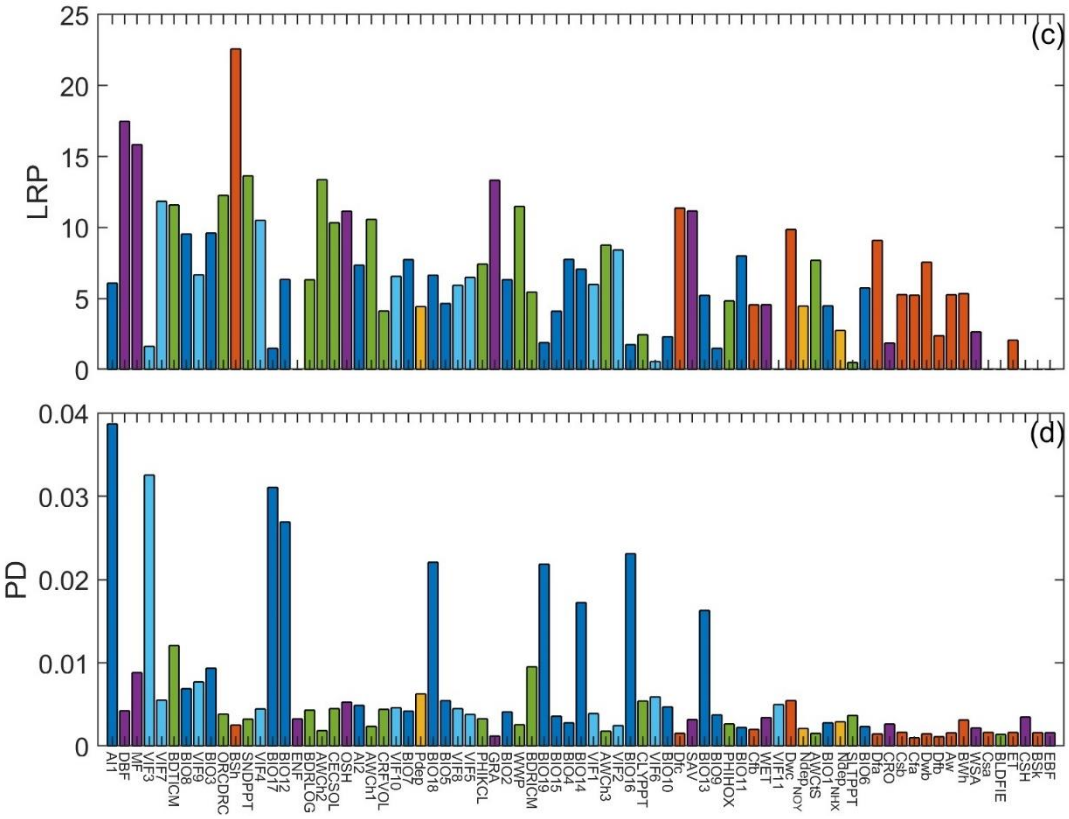

Figure 7. The input features sorted by the average normalized SHAP, LRP and PD for all parameters (a, see definitions in section 2.6). The detailed average SHAP, LRP and PD values for all parameters are displayed in b-d. The features (see definitions in **Table 2**) are classifed into plant functional types (PFT, purple), Koeppen-Geiger climate classification types (Clim, orange), bioclimate variables (BioClim, dark blue), vegetation features (VIF, shallow blue), atmospheric deposition (NPdep, yellow) and soil properties (Soil, green).

4. Discussion

4.1 Well-constrained site-specific parameterization is better than PFT-dependent parameterization

The PFT-based parameterization has been applied for a long time (Running et al., 2004), which was shown cannot capture the variance in parameters within PFT (Bloom et al., 2016) and can introduce the misclassification errors. The method to directly use parameters from papers without local or global evaluation can be also risky. P-model which adopted the globally fixed parameters upscaled from the leaf-scale might not include the PFT errors (Mengoli et al., 2022; Stocker et al., 2020), but had limited accuracy across the temporal (Figure 2) and spatial scales (Figure 3). Actually, our results showed that the globally fixed parameterization methods (e.g., P-model) were worse than PFT-based method (e.g., OPT-PFT, and PFT_{mean}). The globally optimization method (OPT-All) had slightly better performance than PFT-based optimization at the global scale (Figure 5) due to higher spatial generalizability (e.g., Figure 3), the same as Yuan et al (2014), but had accurate prediction at less sites (i.e., less bright blocks in Figure 2). This agrees with a study using PRELES model (Tian et al., 2020), which demonstrated that globally optimized parameters are not sufficient to reflect the variability of the GPP sensitivities. Luo et al (2020) also confirmed that model parameters should vary with the spatial and temporal changes of ecosystem properties. While the site-specific method (PFT_{sim}, sRF, mRF, and mNN-Par) include wider spatial variability than PFT- and climate-type-based method (PFT_{mean}, $Clim_{mean}$, PFT_{med} and $Clim_{med}$), it did not show robust advantage due to uncertainties remained in the calibrated parameters, which were used to constrain the predicted parameters. However, the site-specific parameterization which considers the GPP prediction error, mNN-GPP, reaches the highest performance, highlighting that the well-constrained site-specific parameterization method can provide more reliable outputs than PFT-based method. This is opposite from the conclusion of Tian et al. (2020) which tested only the site-specific optimization method showing higher uncertainties than PFT-based optimization method.

4.2 Reduce parameter uncertainty by considering the relationship between parameters and ecosystem properties

Our results reveal the equifinality of model parameters, which consequently increases the model uncertainty. While no extrapolated parameter vectors outperformed calibrated ones, the parameter ranges were constrained in all methods based on site-specific input features (e.g., sRF, mRF, mNN-Par and mNN-GPP) compared with calibration and optimization methods (see Figure S5-7). It demonstrated that considering the physical links between GPP sensitivities and the ecosystem properties can reduce the parameter uncertainties. This is also true in other LUE models (Horn & Schulz, 2011b). Furthermore, mNN-GPP, considering only the GPP errors but not the distance to calibrated parameters, avoids inheriting uncertainties from model calibration. In general, the model parameterization relying on ecosystem properties can reduce the parameter uncertainty resulted from model equifinality.

4.3 Drivers of the spatial variability of GPP sensitivities

We assume that GPP sensitivities to environmental changes are reflected by the model parameters. The feature importance assessment showed that bioclimate variables, PFT, and vegetation features are controlling the spatial variability of the GPP sensitivities. This is similar to the results of other independent studies using a different LUE model (Horn & Schulz, 2011b) and terrestrial biosphere models (Peaucelle et al., 2019). However, we here used only the variables that represent the climate, vegetation, atmospheric deposition and soil properties. Other unknown important features such as illumination features, which was shown important in Horn et al's study (2011b), were not tested. This might result in insufficient spatial variance in the predicted parameters. Further, we found that the detected important features differed across measuring methods (i.e., SHAP, LRP and PD) and input features (see the result of using a subset of input features which achieve similar accuracy, Figure S10). Several input features are correlated (Figure S11) but not refined. This additionally increase the difficulty to identify the key features determining variability of GPP sensitivities. Besides, the temporal changes in the ecosystem properties can affect the parameters (Luo & Schuur, 2020). To extrapolate parameters to longer time scales (e.g., decades), the temporal variation in parameters needs to be considered.

5. Conclusion

In this study we find a method to parameterize a LUE model based on the link between parameters and ecosystem properties and the distance to observed GPP. This method enables the parameter extrapolation in regions without observational data with a significantly higher accuracy than the widely-used PFT-based and globally fixed parameterization methods. This method can reduce the parameter uncertainty by predicting them using the ecosystem properties without reference of calibrated parameters which usually have high uncertainties. bioclimate variables, PFT, and vegetation features are the most important ecosystem properties controlling the spatial variability of LUE model parameters. The temporal variation in the parameters and the relationship between them and ecosystem properties need to be further explored. Since our parameterization method has high robustness across various temporal and spatial scales, we encourage the application to other GPP models and spatio-temporal scales.

Acknowledgement

This paper is funded by the European Space Agency (ESA) via the Earth System Data Lab (ESDL) project.

References

Bach, S., Binder, A., Montavon, G., Klauschen, F., Müller, K.-R., & Samek, W. (2015). On pixel-wise explanations for non-linear classifier decisions by layer-wise relevance propagation. *Plos One, 10*(7), e0130140.

Baldocchi, D., Ryu, Y., & Keenan, T. (2016). Terrestrial carbon cycle variability. *F1000Research, 5*.

Bao, S., Wutzler, T., Koirala, S., Cuntz, M., Ibrom, A., Besnard, S., . . . Weber, U. (2022). Environment-sensitivity functions for gross primary productivity in light use efficiency models. *Agricultural and Forest Meteorology, 312*, 108708.

Bloom, A. A., Exbrayat, J.-F., Van Der Velde, I. R., Feng, L., & Williams, M. (2016). The decadal state of the terrestrial carbon cycle: Global retrievals of terrestrial carbon allocation, pools, and residence times. *Proceedings of the National Academy of Sciences, 113*(5), 1285-1290.

Breiman, L. (2001). Random forests. *Machine learning, 45*(1), 5-32.

Carvalhais, N., Reichstein, M., Collatz, G., Mahecha, M., Migliavacca, M., Neigh, C., . . . Seixas, J. (2010). Deciphering the components of regional net ecosystem fluxes following a bottom-up approach for the Iberian Peninsula. *Biogeosciences, 7*(11), 3707-3729.

Carvalhais, N., Reichstein, M., Seixas, J., Collatz, G. J., Pereira, J. S., Berbigier, P., . . . Papale, D. (2008). Implications of the carbon cycle steady state assumption for biogeochemical modeling performance and inverse parameter retrieval. *Global Biogeochemical Cycles, 22*(2).

de Sousa, L. M., Poggio, L., Batjes, N. H., Heuvelink, G. B., Kempen, B., Riberio, E., & Rossiter, D. (2020). SoilGrids 2.0: producing quality-assessed soil information for the globe. *Soil Discuss, 1*(10.5194).

Farquhar, G. D., von Caemmerer, S. v., & Berry, J. A. (1980). A biochemical model of photosynthetic CO2 assimilation in leaves of C3 species. *planta, 149*(1), 78-90.

Frankenberg, C., Fisher, J. B., Worden, J., Badgley, G., Saatchi, S. S., Lee, J. E., . . . Kuze, A. (2011). New global observations of the terrestrial carbon cycle from GOSAT: Patterns of plant fluorescence with gross primary productivity. *Geophysical Research Letters, 38*(17).

Friedman, J. H. (2001). Greedy function approximation: a gradient boosting machine. *Annals of statistics*, 1189-1232.

Gardner, M. W., & Dorling, S. (1998). Artificial neural networks (the multilayer perceptron)—a review of applications in the atmospheric sciences. *Atmospheric environment, 32*(14-15), 2627-2636.

Greenwell, B. M., Boehmke, B. C., & McCarthy, A. J. (2018). A simple and effective model-based variable importance measure. *arXiv preprint arXiv:1805.04755*.

Groenendijk, M., Dolman, A., Van der Molen, M., Leuning, R., Arneth, A., Delpierre, N., . . . Verbeeck, H. (2011). Assessing parameter variability in a photosynthesis model within and between plant functional types using global Fluxnet eddy covariance data. *Agricultural and Forest Meteorology, 151*(1), 22-38.

Guan, X., Chen, J. M., Shen, H., Xie, X., & Tan, J. (2022). Comparison of big-leaf and two-leaf light use efficiency models for GPP simulation after considering a radiation scalar. *Agricultural and Forest Meteorology, 313*, 108761.

Hansen, N., & Kern, S. (2004). *Evaluating the CMA evolution strategy on multimodal test functions.* Paper presented at the International conference on parallel problem solving from nature.

He, M., Ju, W., Zhou, Y., Chen, J., He, H., Wang, S., . . . Li, Y. (2013). Development of a two-leaf light use efficiency model for improving the calculation of terrestrial gross primary productivity. *Agricultural and Forest Meteorology, 173*, 28-39.

Horn, J., & Schulz, K. (2011a). Identification of a general light use efficiency model for gross primary production. *Biogeosciences, 8*(4), 999-1021.

Horn, J., & Schulz, K. (2011b). Spatial extrapolation of light use efficiency model parameters to predict gross primary production. *Journal of Advances in Modeling Earth Systems, 3*(4).

Huntzinger, D. N., Michalak, A. M., Schwalm, C., Ciais, P., King, A. W., Fang, Y., . . . Zhao, F. (2017). Uncertainty in the response of terrestrial carbon sink to environmental drivers undermines carbon-climate feedback predictions. *Scientific Reports, 7*(1), 4765. Retrieved from https://doi.org/10.1038/s41598-017-03818-2. doi:10.1038/s41598-017-03818-2

Jung, M., Reichstein, M., Margolis, H. A., Cescatti, A., Richardson, A. D., Arain, M. A., . . . Chen, J. (2011). Global patterns of land-atmosphere fluxes of carbon dioxide, latent heat, and sensible heat derived from eddy covariance, satellite, and meteorological observations. *Journal of Geophysical Research: Biogeosciences, 116*(G3).

Kalliokoski, T., Makela, A., Fronzek, S., Minunno, F., & Peltoniemi, M. (2018). Decomposing sources of uncertainty in climate change projections of boreal forest primary production. *Agricultural and Forest Meteorology, 262*, 192-205. Retrieved from <Go to ISI>://WOS:000444659300018. doi:10.1016/j.agrformet.2018.06.030

Kingma, D. P., & Ba, J. (2014). Adam: A method for stochastic optimization. *arXiv preprint arXiv:1412.6980*.

Lundberg, S. M., & Lee, S.-I. (2017, 2017

Dec 04-09). *A Unified Approach to Interpreting Model Predictions.* Paper presented at the 31st Annual Conference on Neural Information Processing Systems (NIPS), Long Beach, CA.

Luo, Y., & Schuur, E. A. G. (2020). Model parameterization to represent processes at unresolved scales and changing properties of evolving systems. *Global change biology, 26*(3), 1109-1117. Retrieved from <Go to ISI>://WOS:000506663700001. doi:10.1111/gcb.14939

Mahadevan, P., Wofsy, S. C., Matross, D. M., Xiao, X., Dunn, A. L., Lin, J. C., . . . Gottlieb, E. W. (2008). A satellite‐based biosphere parameterization for net ecosystem CO2 exchange: Vegetation Photosynthesis and Respiration Model (VPRM). *Global Biogeochemical Cycles, 22*(2).

Mäkelä, A., Pulkkinen, M., Kolari, P., Lagergren, F., Berbigier, P., Lindroth, A., . . . Hari, P. (2008). Developing an empirical model of stand GPP with the LUE approach: analysis of eddy covariance data at five contrasting conifer sites in Europe. *Global change biology, 14*(1), 92-108.

McCulloch, W. S., & Pitts, W. (1943). A logical calculus of the ideas immanent in nervous activity. *The bulletin of mathematical biophysics, 5*(4), 115-133.

Medlyn, B. E., Robinson, A. P., Clement, R., & McMurtrie, R. E. (2005). On the validation of models of forest CO2 exchange using eddy covariance data: some perils and pitfalls. *Tree Physiology, 25*(7), 839-857. Retrieved from https://doi.org/10.1093/treephys/25.7.839. doi:10.1093/treephys/25.7.839

Mengoli, G., Agusti-Panareda, A., Boussetta, S., Harrison, S. P., Trotta, C., & Prentice, I. C. (2022). Ecosystem Photosynthesis in Land-Surface Models: A First-Principles Approach Incorporating Acclimation. *Journal of Advances in Modeling Earth Systems, 14*(1). Retrieved from <Go to ISI>://WOS:000751889900010. doi:10.1029/2021ms002767

Montavon, G., Binder, A., Lapuschkin, S., Samek, W., & Müller, K.-R. (2019). Layer-wise relevance propagation: an overview. *Explainable AI: interpreting, explaining and visualizing deep learning*, 193-209.

Monteith, J. (1972). Solar radiation and productivity in tropical ecosystems. *Journal of applied ecology, 9*(3), 747-766.

Peaucelle, M., Bacour, C., Ciais, P., Vuichard, N., Kuppel, S., Peñuelas, J., . . . Chen, J. (2019). Covariations between plant functional traits emerge from constraining parameterization of a terrestrial biosphere model. *Global ecology and biogeography, 28*(9), 1351-1365.

Pedregosa, F., Varoquaux, G., Gramfort, A., Michel, V., Thirion, B., Grisel, O., . . . Dubourg, V. (2011). Scikit-learn: Machine learning in Python. *the Journal of machine Learning research, 12*, 2825-2830.

Piao, S., Wang, X., Wang, K., Li, X., Bastos, A., Canadell, J. G., . . . Sitch, S. (2020). Interannual variation of terrestrial carbon cycle: Issues and perspectives. *Global change biology, 26*(1), 300-318.

Potter, C. S., Randerson, J. T., Field, C. B., Matson, P. A., Vitousek, P. M., Mooney, H. A., & Klooster, S. A. (1993). Terrestrial ecosystem production: a process model based on global satellite and surface data. *Global Biogeochemical Cycles, 7*(4), 811-841.

Prentice, I. C., Dong, N., Gleason, S. M., Maire, V., & Wright, I. J. (2014). Balancing the costs of carbon gain and water transport: testing a new theoretical framework for plant functional ecology. *Ecology letters, 17*(1), 82-91.

Running, S. W., Nemani, R. R., Heinsch, F. A., Zhao, M., Reeves, M., & Hashimoto, H. (2004). A continuous satellite-derived measure of global terrestrial primary production. *Bioscience, 54*(6), 547-560.

Ryu, Y., Berry, J. A., & Baldocchi, D. D. (2019). What is global photosynthesis? History, uncertainties and opportunities. *Remote Sensing of Environment, 223*, 95-114. Retrieved from https://www.sciencedirect.com/science/article/pii/S0034425719300161. doi:https://doi.org/10.1016/j.rse.2019.01.016

Srivastava, N., Hinton, G., Krizhevsky, A., Sutskever, I., & Salakhutdinov, R. (2014). Dropout: A Simple Way to Prevent Neural Networks from Overfitting. *Journal of Machine Learning Research, 15*, 1929-1958. Retrieved from <Go to ISI>://WOS:000344638300002.

Stocker, B. D., Wang, H., Smith, N. G., Harrison, S. P., Keenan, T. F., Sandoval, D., . . . Prentice, I. C. (2020). P-model v1. 0: an optimality-based light use efficiency model for simulating ecosystem gross primary production. *Geoscientific Model Development, 13*(3), 1545-1581.

Tian, X., Minunno, F., Cao, T., Peltoniemi, M., Kalliokoski, T., & Mäkelä, A. (2020). Extending the range of applicability of the semi-empirical ecosystem flux model PRELES for varying forest types and climate. *Global change biology, 26*(5), 2923-2943.

Viovy, N. (2018). CRUNCEP version 7-atmospheric forcing data for the community land model. *Research Data Archive at the National Center for Atmospheric Research, Computational and Information Systems Laboratory, 10*.

Walther, S., Besnard, S., Nelson, J. A., El-Madany, T. S., Migliavacca, M., Weber, U., . . . Jung, M. (2022). Technical note: A view from space on global flux towers by MODIS and Landsat: the FluxnetEO data set. *Biogeosciences, 19*(11), 2805-2840. Retrieved from <Go to ISI>://WOS:000807411900001. doi:10.5194/bg-19-2805-2022

Wang, H., Prentice, I. C., Keenan, T. F., Davis, T. W., Wright, I. J., Cornwell, W. K., . . . Peng, C. (2017). Towards a universal model for carbon dioxide uptake by plants. *Nature plants, 3*(9), 734-741.

Wang, R., Goll, D., Balkanski, Y., Hauglustaine, D., Boucher, O., Ciais, P., . . . Sardans, J. (2017). Global forest carbon uptake due to nitrogen and phosphorus deposition from 1850 to 2100. *Global change biology, 23*(11), 4854-4872.

Xiao, X., Hollinger, D., Aber, J., Goltz, M., Davidson, E. A., Zhang, Q., & Moore III, B. (2004). Satellite-based modeling of gross primary production in an evergreen needleleaf forest. *Remote Sensing of Environment, 89*(4), 519-534.

Xie, X., & Li, A. (2020). An adjusted two-leaf light use efficiency model for improving GPP simulations over mountainous areas. *Journal of Geophysical Research: Atmospheres, 125*(13), e2019JD031702.

Xu, T., & Hutchinson, M. (2011). ANUCLIM version 6.1 user guide. *The Australian National University, Fenner School of Environment and Society, Canberra, 90*.

Yan, H., Wang, S. Q., Yu, K. L., Wang, B., Yu, Q., Bohrer, G., . . . Shugart, H. H. (2017). A novel diffuse fraction-based two-leaf light use efficiency model: An application quantifying photosynthetic seasonality across 20 AmeriFlux flux tower sites. *Journal of Advances in Modeling Earth Systems, 9*(6), 2317-2332.

Yuan, W., Cai, W., Liu, S., Dong, W., Chen, J., Arain, M. A., . . . Georgiadis, T. (2014). Vegetation-specific model parameters are not required for estimating gross primary production. *Ecological modelling, 292*, 1-10.

Yuan, W., Cai, W., Xia, J., Chen, J., Liu, S., Dong, W., . . . Beringer, J. (2014). Global comparison of light use efficiency models for simulating terrestrial vegetation gross primary production based on the LaThuile database. *Agricultural and Forest Meteorology, 192*, 108-120.

Yuan, W., Liu, S., Zhou, G., Zhou, G., Tieszen, L. L., Baldocchi, D., . . . Goulden, M. L. (2007). Deriving a light use efficiency model from eddy covariance flux data for predicting daily gross primary production across biomes. *Agricultural and Forest Meteorology, 143*(3-4), 189-207.

Yuan, W., Zheng, Y., Piao, S., Ciais, P., Lombardozzi, D., Wang, Y., . . . Hu, Z. (2019). Increased atmospheric vapor pressure deficit reduces global vegetation growth. *Science advances, 5*(8), eaax1396.

Zhang, F., Chen, J. M., Chen, J., Gough, C. M., Martin, T. A., & Dragoni, D. (2012). Evaluating spatial and temporal patterns of MODIS GPP over the conterminous US against flux measurements and a process model. *Remote Sensing of Environment, 124*, 717-729.

Zheng, Y., Shen, R., Wang, Y., Li, X., Liu, S., Liang, S., . . . Yuan, W. (2020). Improved estimate of global gross primary production for reproducing its long-term variation, 1982–2017. *Earth System Science Data, 12*(4), 2725-2746.

Zheng, Y., Zhang, L., Xiao, J., Yuan, W., Yan, M., Li, T., & Zhang, Z. (2018). Sources of uncertainty in gross primary productivity simulated by light use efficiency models: Model structure, parameters, input data, and spatial resolution. *Agricultural and Forest Meteorology, 263*, 242-257.

Zhou, Y., Wu, X., Ju, W., Chen, J. M., Wang, S., Wang, H., . . . Ibrom, A. (2016). Global parameterization and validation of a two-leaf light use efficiency model for predicting gross primary production across FLUXNET sites. *Journal of Geophysical Research: Biogeosciences, 121*(4), 1045-1072.